LETTER

Perovskite/Perovskite Tandem Solar Cells in the Substrate Configuration with Potential for Bifacial Operation

Lidón Gil-Escrig,[||] Shuaifeng Hu,[||] Kassio P. S. Zanoni, Abhyuday Paliwal, M. Angeles Hernández-Fenollosa, Cristina Roldán-Carmona, Michele Sessolo, Atsushi Wakamiya, and Henk J. Bolink*

Read Online

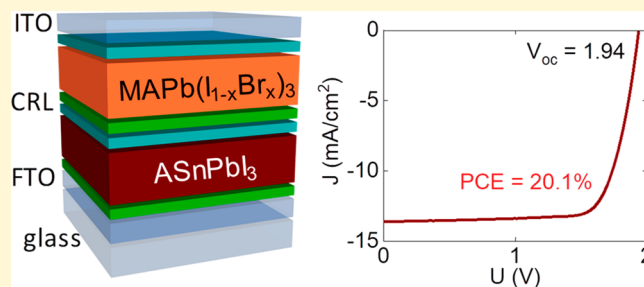| ACCESS | | � 📊 Metrics & More | | 📖 Article Recommendations | | 🆂🅸 Supporting Information |

ABSTRACT: Perovskite/perovskite tandem solar cells have recently exceeded the record power conversion efficiency (PCE) of single-junction perovskite solar cells. They are typically built in the superstrate configuration, in which the device is illuminated from the substrate side. This limits the fabrication of the solar cell to transparent substrates, typically glass coated with a transparent conductive oxide (TCO), and adds constraints because the first subcell that is deposited on the substrate must contain the wide-bandgap perovskite. However, devices in the substrate configuration could potentially be fabricated on a large variety of opaque and inexpensive substrates, such as plastic and metal foils. Importantly, in the substrate configuration the narrow-bandgap subcell is deposited first, which allows for more freedom in the device design. In this work, we report perovskite/perovskite tandem solar cells fabricated in the substrate configuration. As the substrate we use TCO-coated glass on which a solution-processed narrow-bandgap perovskite solar cell is deposited. All of the other layers are then processed using vacuum sublimation, starting with the charge recombination layers, then the wide-bandgap perovskite subcell, and finishing with the transparent top TCO electrode. Proof-of-concept tandem solar cells show a maximum PCE of 20%, which is still moderate compared to those of best-in-class devices realized in the superstrate configuration yet higher than those of the corresponding single-junction devices in the substrate configuration. As both the top and bottom electrodes are semitransparent, these devices also have the potential to be used as bifacial tandem solar cells.
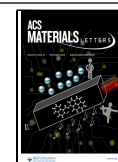
T hin-film solar cells based on metal halide perovskites have rapidly evolved into one of the most promising photovoltaic (PV) technologies, reaching record efficiencies for single-junction devices exceeding 25.5%.[1,2] While remarkable, this value is close to the maximum achievable power conversion efficiency (PCE) for a 1.5 eV bandgap semiconductor.[3] One way to overcome this limit is the development of multijunction perovskite solar cells, which is possible thanks to the inherent bandgap tunability of metal halide perovskites.[4−7] Double-junction (tandem) perovskite devices are either monolithic (or two-terminal, 2T) or employ two individual subcells with four terminals (4T). In 4T tandem solar cells, the wide-bandgap subcell must be semitransparent, yet due to the trade-off in conductivity and transmission some optical losses are inevitable. In the 2T configuration, the two subcells are connected via a charge recombination layer (CRL). 2T perovskite tandem cells that are being investigated are based on perovskite/perovskite,[8−14] perovskite with

CIGS[15,16] or even with organic semiconductors,[17] and perovskite/silicon,[18−23] which have demonstrated PCEs approaching 30%.[21,23] Perovskite/perovskite tandem solar cells have recently exceeded the record PCE of single-junction perovskite solar cells,[24] with reported PCEs of up to 28%,[25] and are particularly interesting because they can be prepared on lightweight and flexible substrates.[26] The most efficient perovskite single-junction and perovskite/perovskite tandem solar cells are built in the superstrate configuration, in which the device is illuminated from the substrate side. This limits the
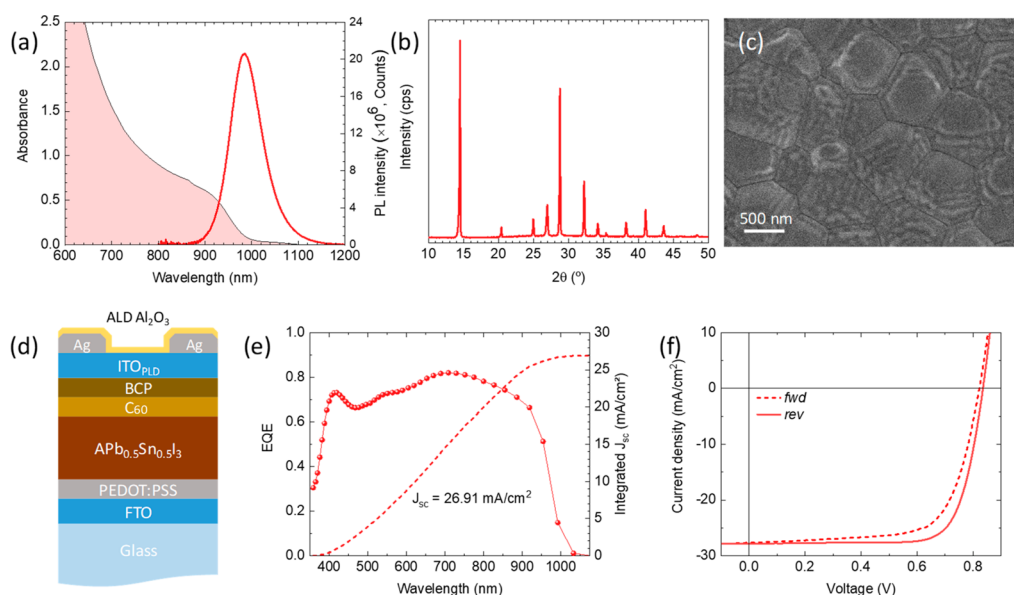
Figure 1. (a) Absorbance (left, colored area) and PL (right, red line) spectra obtained under laser excitation at 688 nm for a $Cs_{0.1}FA_{0.6}MA_{0.3}Pb_{0.5}Sn_{0.5}I_3$ perovskite film. (b) XRD pattern and (c) SEM surface morphology of the same material. (d) Device structure (A = $Cs_{0.1}FA_{0.6}MA_{0.3}$), (e) EQE spectrum with integrated short-circuit current density, and (f) $J-V$ curves under simulated solar illumination recorded in forward and reverse scan directions. Both (e) and (f) were measured by illuminating the device through the top ITO_{PLD} contact.

fabrication of the solar cell to transparent substrates, typically glass coated with a transparent conductive oxide (TCO).[27] Additionally, it implies that the first perovskite subcell that is deposited on the TCO must contain the wide-bandgap perovskite and the second subcell that is deposited on top of the CRL must be the narrow-bandgap cell. Tandem perovskite devices with Si or CIGS are built in the substrate configuration using a nontransparent substrate (Si or CIGS in this case) and a transparent top electrode, most commonly a TCO.[28] Research on perovskite solar cells in the substrate configuration has been mainly focused on the development of near-infrared (NIR) transparent devices for 4T tandem applications.[29] However, devices in the substrate configuration could potentially be fabricated on a large variety of opaque and inexpensive substrates, such as plastic and metal foils, for building integrated PVs.[30−32] Importantly, in the substrate configuration the narrow-bandgap subcell is deposited first, which allows for more freedom in the device design. The first proof-of-concept all-perovskite tandem solar cell in the substrate configuration with an efficiency of 18% was reported by Werner et al.[33] In that first example, however, details of the device fabrication and characterization were not reported.

Here we describe in detail the fabrication and characterization of perovskite/perovskite tandem solar cells fabricated in the substrate configuration. As the substrate we use TCO-coated glass on which a solution-processed narrow-bandgap (Sn−Pb) perovskite solar cell is deposited. All of the other layers are then processed using vacuum sublimation, starting with the charge recombination layers (CRLs), then the wide-bandgap perovskite subcell, and finishing with the TCO top electrode. Proof-of-concept tandem solar cells show a maximum PCE of 20%, which is still moderate compared to those of best-in-class devices realized in the superstrate configuration yet higher than those of the reference single-junction Sn−Pb devices in the substrate configuration (with PCEs of up to 17.5%). As both the top and bottom electrodes

are semitransparent, these devices could also be used as bifacial tandem solar cells.[34]

Multication mixed Sn−Pb narrow-bandgap perovskite films of nominal composition $Cs_{0.1}FA_{0.6}MA_{0.3}Pb_{0.5}Sn_{0.5}I_3$ (MA = methylammonium; FA = formamidinium) were solution-processed using a protocol recently reported by some of us.[35] Briefly, glass substrates coated with fluorine-doped tin oxide (FTO) were cleaned and coated with poly(3,4-ethylenedioxythiophene):poly(styrenesulfonate) (PE-DOT:PSS). A 1.8 M precursor solution containing PbI_2, SnI_2, CsI, FAI, and MAI prepared in 3:1 v/v N,N-dimethylformamide/dimethyl sulfoxide was used. SnF_2 (10 mol % with respect to SnI_2) and NH_4SCN (2 mol % with respect to the total amount of B-site precursor, SnI_2 + PbI_2) were added to the perovskite precursor solution to suppress Sn(II) oxidation and mediate the perovskite crystallization, respectively. Glycine hydrochloride (GlyHCl) (2 mol % with respect to the total amount of B-site precursor) was added to the precursor solution to modify the bottom interface, while for top interface modification a solution of ethylenediammonium iodide ($EDAI_2$) in 1:1 v/v isopropanol/toluene was spin-coated on the top of the perovskite films. The as-prepared Sn−Pb films have an optical absorption onset at approximately 1000 nm (Figure 1a) and a photoluminescence (PL) peak centered at 984 nm, corresponding to an optical bandgap energy (E_g) of 1.26 eV. The X-ray diffraction (XRD) pattern obtained for the Sn−Pb perovskite films (Figure 1b) shows the expected perovskite pattern, with reflections at 2θ values of 14.2°, 20.1°, 24.6°, 28.4°, 31.9°, 35.0°, 40.7°, and 43.2°, corresponding to the (100), (110), (111), (200), (210), (211), (220), and (300) planes, respectively.[35] No unreacted PbI_2 could be observed, as the reflection at $2\theta = 12.7°$ is absent. The surface morphology as observed by scanning electron microscopy (SEM) (Figure 1c) shows large grains (diameters between 0.5 and 1.0 μm) arranged in a compact fashion without visible voids or superstructures.
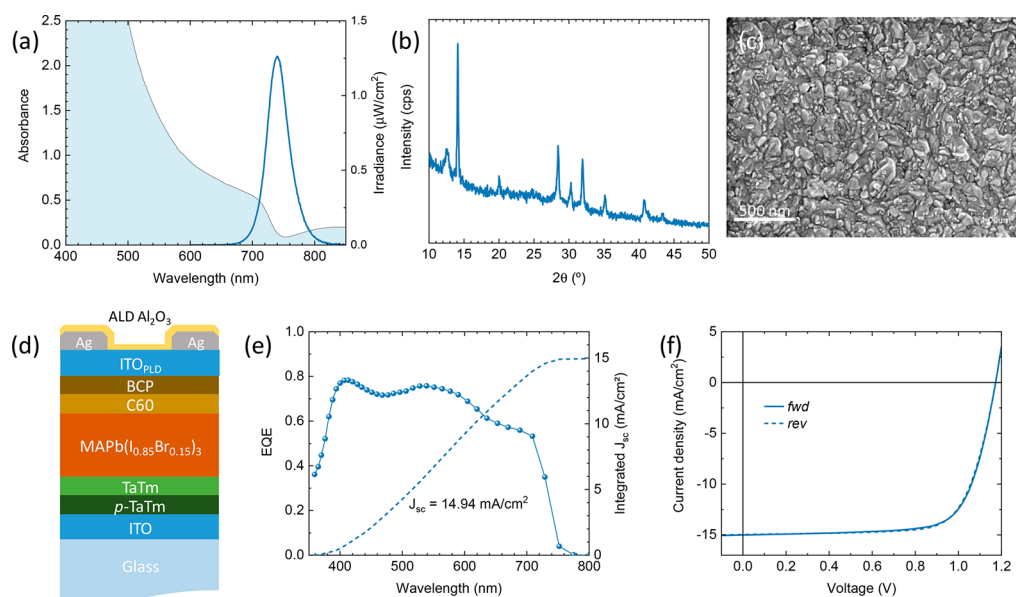
Figure 2. (a) Absorbance (left, colored area) and PL (right, blue line) spectra obtained under laser excitation at 522 nm for a MAPb($I_{0.85}Br_{0.15})_3$ perovskite film. (b) XRD pattern and (c) SEM surface morphology of the same material. (d) Device structure, (e) EQE spectrum with integrated short-circuit current, and (f) $J-V$ curves under simulated solar illumination recorded in the forward and reverse scan directions. Both (e) and (f) were measured by illuminating the device through the top ITO_{PLD} contact.

We prepared solar cells in the substrate configuration shown in Figure 1d using the $Cs_{0.1}FA_{0.6}MA_{0.3}Pb_{0.5}Sn_{0.5}I_3$ perovskite film. Glass/FTO/PEDOT:PSS/perovskite samples were coated with C_{60} fullerene (20 nm) and shipped from Kyoto to Valencia in a vacuum-sealed transport chamber (typical shipping time 3−4 days) that was opened in a nitrogen-filled glovebox. Bathocuproine (BCP) (7 nm) was sublimed in a vacuum chamber integrated into the glovebox. Indium tin oxide (ITO) was directly deposited by pulsed laser deposition (PLD) (ITO_{PLD}) on top of the BCP layer through a shadow mask using a low-damage protocol recently developed by some of us.[36] To ensure maximum current collection and minimize resistance losses, thin (100 nm) silver grid lines were vacuum-deposited on the sides of the PLD_{ITO} contacts (details are provided in the Supporting Information). The solar cells were encapsulated with a 20 nm thick Al_2O_3 film deposited by atomic layer deposition (ALD).[37] All of the device characterization was carried out by illuminating the solar cells through the ITO_{PLD} in the substrate configuration. The external quantum efficiency (EQE) spectrum of the Sn−Pb perovskite solar cells (Figure 1e) shows a cutoff at approximately 1000 nm and increases to >0.8 at 700 nm. The EQE minimum in the UV−visible part of the spectrum (400−600 nm) is a consequence of the optical absorption of the fullerene, which is used as the electron transport layer (ETL). From the first-order derivative of the EQE spectrum (Figure S1), we estimated an E_g value of 1.28 eV, similar to what was observed by PL. The integrated current density (26.9 mA/cm²) agrees well with the short-circuit current density (J_{sc}) measured with current density versus voltage ($J-V$) scans under simulated solar illumination (Figure 1f). Statistics of the characteristic PV parameters are reported in Figure S2. We observed hysteresis between $J-V$ curves collected in the forward (*fwd*, from short- to open-circuit) and reverse (*rev*, from open- to short-circuit) bias directions. The open-circuit voltage (V_{oc}) and J_{sc} were found to improve only marginally from 0.82 to 0.83 V and 27.2 to 27.6 mA/cm², respectively, when the bias direction was

changed from forward to reverse. The main difference was found in the fill factor (FF), which increased on average from 67.5% to 74.9% for scanning in the forward and reverse bias directions, respectively. This results in average PCEs of 15.1% and 17.2% estimated from the forward and reverse $J-V$ scans, respectively. We noticed that the performance of the device is lower when it is measured through the top ITO compared to measurements with illumination through the substrate side (Figure S3). This difference is likely related to the presence of the absorbing C_{60}, as the main limiting parameter is J_{sc} (from the glass side it is as high as 29 mA/cm²). The record semitransparent pixel measured through the top ITO delivered a PCE of 17.7% in the reverse scan.

We then prepared vacuum-deposited wide-bandgap perovskites of the type MAPb($I_{0.85}Br_{0.15})_3$ by three-source deposition from MAI, PbI_2, and $PbBr_2$ following a previously reported protocol.[38] The as-prepared MAPb($I_{0.85}Br_{0.15})_3$ films show an optical absorption onset at approximately 740 nm (Figure 2a; the sub-bandgap band is due to interference and not to optical absorption by the perovskite—see Figure S4 for the full spectrum) and a PL peak centered at 740 nm, corresponding to an optical E_g of 1.68 eV. The XRD pattern of the wide-bandgap perovskite films is compatible with a cubic perovskite (Figure 2b) with some residual PbI_2, as indicated from the reflection at $2\theta = 12.7°$. The signal-to-noise ratio of the XRD pattern was found to be rather low, which might be related to the low crystallinity of the films as observed by SEM (Figure 2c), which shows small and randomly oriented grains with a compact surface morphology.

We prepared solar cells in the substrate configuration depicted in Figure 2d. The device structure is ITO/TaTm:F_6-TCNNQ (25 nm)/TaTm (10 nm)/MAPb($I_{0.85}Br_{0.15})_3$ (450 nm)/C_{60} (25 nm)/BCP (8 nm)/ITO_{PLD}, where TaTm is N4,N4,N4″,N4″-tetrakis([1,1′-biphenyl]-4-yl)-[1,1′:4′,1″-terphenyl]-4,4″-diamine) and F_6-TCNNQ is 2,2′-(perfluoronaphthalene-2,6-diylidene)dimalononitrile. The notation TaTm:F_6-TCNNQ indicates that the two materials are cosublimed (F_6-
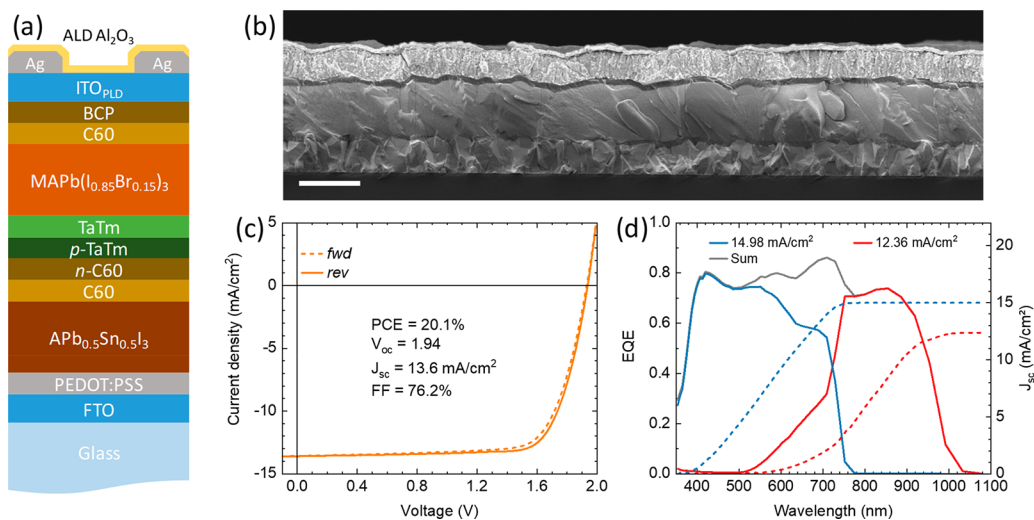
Figure 3. (a) Tandem device structure, where A = $Cs_{0.1}FA_{0.6}MA_{0.3}$, n-C_{60} refers to C_{60} cosublimed with the n-dopant PhIm, and p-TaTm refers to TaTm cosublimed with the p-dopant F_6-TCNNQ. (b) SEM cross-section of the full tandem device (scale bar is 1 μm). (c) $J–V$ curves under simulated solar illumination recorded in the forward and reverse scan directions. (d) EQE spectra of the tandem device with integrated short-circuit currents for both subcells. The EQE spectra of the two subcells are reported together with their sum. (c) and (d) were measured by illuminating the device through the top ITO_{PLD} contact.

TCNNQ at 10 wt %) in order to increase the conductivity of the film, which is used as the hole injection layer (HIL).[39] The solar cells were encapsulated with an ALD Al_2O_3 coating and measured by illuminating through the top ITO_{PLD} in the substrate configuration. The EQE spectrum of the MAPb-$(I_{0.85}Br_{0.15})_3$ perovskite solar cells (Figure 2e) shows a cutoff at approximately 750 nm and increases to 0.75 at 560 nm. Again, the EQE minimum in the 400−500 nm range is a consequence of the optical absorption of the fullerene ETL. From the first-order derivative of the EQE (Figure S5), we estimated an E_g value of 1.69 eV, similar to what was observed by PL. The integrated current density (14.94 mA/cm²) agrees well with the J_{sc} measured with the $J–V$ scans under simulated solar illumination (Figure 2f). The $J–V$ scans showed virtually no hysteresis between the forward and reverse scans, which suggests that ion migration and/or interface recombination are suppressed in these perovskite solar cells.[40,41] On average, the J_{sc}, V_{oc}, and FF were found to be 14.8 ± 0.4 mA/cm², 1.17 ± 0.01 V, and 73.2 ± 1.0, respectively, resulting in a PCE of 12.6 ± 0.1%. These parameters agree with previous reports on similar vacuum-deposited solar cells, apart from the J_{sc} value, which is lower due to incomplete absorption by the perovskite stack.[38] The lower photocurrent is a consequence of the reduced perovskite thickness, which was selected on purpose to target roughly half of the current density produced by the Sn−Pb solar cells (28−29 mA/cm²) in order to achieve current matching in the tandem configuration. It should be noted that this is a first rough estimation. One should choose a top cell thickness so that it delivers the same current density as the bottom cell, when the latter is filtered by the very same top cell. We also measured the same cells by illuminating them through the glass side (Figure S6). In this case, we found the performance and in particular the current density to be independent of the illumination side, in contrast with what was observed for the narrow-band solar cells (Figure S3). This behavior might arise from different light incoupling through the bottom substrate that compensates for the parasitic absorption of the fullerene when the sample is illuminated from the top ITO electrode.

2T tandem devices in the substrate configuration were prepared following the structure reported in Figure 3a. The narrow-bandgap Sn−Pb perovskite subcells were fabricated up to the C_{60} ETL (without top electrode) in Kyoto as described above and shipped to Valencia for the tandem fabrication and characterization. We used a previously developed CRL based on doped and intrinsic organic semiconductors.[42,43] The CRL consists of a junction between an n-doped C_{60} layer and a p-doped TaTm film (both 25 nm thick). Doping of C_{60} was attained by cosublimation with $N1,N4$-bis(tri-p-tolylphosphoranylidene)benzene-1,4-diamine (PhIm) at 40 wt %. A 10 nm thick TaTm film was then used to reduce charge recombination, and the top wide-bandgap subcell was deposited as described above. As can be seen from Figure 3b, the vacuum-deposited organic CRL (C_{60}/n-C_{60}/p-TaTm/ TaTm) and the top wide-bandgap perovskite cell are conformally coated on the somewhat rough surface of the bottom Sn−Pb perovskite solar cell. The thicknesses of the perovskite layers were approximately 850 and 450 nm for the Sn−Pb and wide-bandgap subcells, respectively, as observed by SEM (details are provided in Figure S7). From the SEM results, the difference in the morphologies of the two perovskites can also be appreciated. The bottom Sn−Pb perovskite appears to be highly homogeneous and crystalline, while the top $MAPb(I_{0.85}Br_{0.15})_3$ layer seems to be more disordered and formed by a compact array of small grains. The $J–V$ curves under illumination for the record solar cell measured in this work (average values are given in Figure S5) showed only a small hysteresis between the forward and reverse bias scans, mainly in the FF (74.3% and 76.2% in the forward and reverse bias directions, respectively). In reverse bias, we measured a PCE of 20.1% for the tandem solar cell in the substrate configuration, which is 2.5% absolute points higher compared to the semitransparent Sn−Pb single-junction solar cell measured in the substrate configuration.

The V_{oc} of the solar cells was measured to be 1.94 V, which is close the expected value of approximately 2.0 V given by the sum of the average V_{oc} values of the two subcells (1.17 and 0.83 V). The photocurrent of the tandem solar cells was found

to be close to the expected value (half of the average J_{sc} of the Sn−Pb perovskite cell, 27.5 mA/cm^2; Figure S2a), with a maximum J_{sc} of 13.6 mA/cm^2. When measuring the EQEs of the subcells constituting the tandem devices, we found the narrow-bandgap Sn−Pb subcell to be limiting the tandem performance. The corresponding integrated current density is only 12.36 mA/cm^2, whereas the wide-bandgap solar cell can deliver 14.98 mA/cm^2. The lower integrated current density measured for the Sn−Pb perovskite compared to the tandem solar cell might be associated with some degree of shunts in the same subcells and by an uncorrected mismatch factor among the two subcells.[44] The initial shelf life device stability was evaluated for samples stored in the dark under a nitrogen atmosphere. After 120 h, the PCE was found to drop only marginally to an average value of 19.5% (Figure S9), which is promising considering the nature and complexity of these devices.

In summary, we show proof-of-concept all-perovskite 2T tandem cells in the substrate configuration. The devices are fabricated using a solution-processed narrow-bandgap $Cs_{0.1}FA_{0.6}MA_{0.3}Pb_{0.5}Sn_{0.5}I_3$ perovskite in the bottom cell and a vacuum-deposited wide-bandgap $MAPb(I_{0.85}Br_{0.15})_3$ perovskite in the top cell. All of the transport layers as well as the charge recombination layers are prepared by vacuum deposition using a combination of intrinsic and doped organic semiconductors. The top transparent electrode (indium tin oxide) is directly deposited onto the thin organic transport layers without the use of a metal oxide buffer thanks to the use of a previously developed soft pulsed laser deposition process. Tandem cells are prepared and characterized in the substrate configuration, obtaining promising efficiencies of up to 20%, surpassing the efficiency of the corresponding single-junction devices also measured in the substrate configuration. As both electrodes are semitransparent, these devices can also be operated as bifacial cells. We are working on a measurement setup to analyze and optimize these tandem solar cells in the bifacial configuration in future work.

■ ASSOCIATED CONTENT

Ⓢ Supporting Information

The Supporting Information is available free of charge at https://pubs.acs.org/doi/10.1021/acsmaterialslett.2c01001.

Experimental section and Figures S1−S9 (PDF)

■ AUTHOR INFORMATION

Corresponding Author

Henk J. Bolink − *Instituto de Ciencia Molecular, Universidad de Valencia, 46980 Paterna, Spain;* ⓞ orcid.org/0000-0001-9784-6253; Email: henk.bolink@uv.es

Authors

Lidón Gil-Escrig − *Instituto de Ciencia Molecular, Universidad de Valencia, 46980 Paterna, Spain*

Shuaifeng Hu − *Institute for Chemical Research, Kyoto University, Uji, Kyoto 611-0011, Japan;* ⓞ orcid.org/0000-0003-1312-075X

Kassio P. S. Zanoni − *Instituto de Ciencia Molecular, Universidad de Valencia, 46980 Paterna, Spain*

Abhyuday Paliwal − *Instituto de Ciencia Molecular, Universidad de Valencia, 46980 Paterna, Spain*

M. Angeles Hernández-Fenollosa − *Instituto de Tecnología de Materiales, Universitat Politècnica de Valencia, 46022 Valencia, Spain*

Cristina Roldán-Carmona − *Instituto de Ciencia Molecular, Universidad de Valencia, 46980 Paterna, Spain*

Michele Sessolo − *Instituto de Ciencia Molecular, Universidad de Valencia, 46980 Paterna, Spain;* ⓞ orcid.org/0000-0002-9189-3005

Atsushi Wakamiya − *Institute for Chemical Research, Kyoto University, Uji, Kyoto 611-0011, Japan;* ⓞ orcid.org/0000-0003-1430-0947

Complete contact information is available at:
https://pubs.acs.org/10.1021/acsmaterialslett.2c01001

Author Contributions

‖L.G.-E. and S.H. contributed equally to this work. CRediT: **Lidon Gil-Escrig** data curation, investigation, methodology, writing-review & editing; **Shuaifeng Hu** data curation, investigation, methodology, writing-review & editing; **Kassio P.S. Zanoni** methodology; **Abhyuday Paliwal** methodology; **M. Ángeles Hernández-Fenollosa** methodology; **Cristina Roldán-Carmona** methodology; **Michele Sessolo** formal analysis, investigation, writing-original draft, writing-review & editing; **Atsushi Wakamiya** resources, supervision, writing-review & editing; **Henk J. Bolink** conceptualization, funding acquisition, resources, supervision, writing-review & editing.

Notes

The authors declare no competing financial interest.

■ ACKNOWLEDGMENTS

■ REFERENCES

(1) Jeong, J.; Kim, M.; Seo, J.; Lu, H.; Ahlawat, P.; Mishra, A.; Yang, Y.; Hope, M. A.; Eickemeyer, F. T.; Kim, M.; et al. Pseudo-Halide Anion Engineering for α-FAPbI$_3$ Perovskite Solar Cells. *Nature* **2021**, *592*, 381−385.

(2) Min, H.; Lee, D. Y.; Kim, J.; Kim, G.; Lee, K. S.; Kim, J.; Paik, M. J.; Kim, Y. K.; Kim, K. S.; Kim, M. G.; et al. Perovskite Solar Cells with Atomically Coherent Interlayers on SnO_2 Electrodes. *Nature* **2021**, *598*, 444−450.

(3) Rühle, S. Tabulated Values of the Shockley−Queisser Limit for Single Junction Solar Cells. *Sol. Energy* **2016**, *130*, 139−147.

(4) Hao, F.; Stoumpos, C. C.; Chang, R. P. H.; Kanatzidis, M. G. Anomalous Band Gap Behavior in Mixed Sn and Pb Perovskites Enables Broadening of Absorption Spectrum in Solar Cells. *J. Am. Chem. Soc.* **2014**, *136*, 8094−8099.

(5) Rajagopal, A.; Stoddard, R. J.; Hillhouse, H. W.; Jen, A. K.-Y. On Understanding Bandgap Bowing and Optoelectronic Quality in Pb−Sn Alloy Hybrid Perovskites. *J. Mater. Chem. A* **2019**, *7*, 16285−16293.

(6) Noh, J. H.; Im, S. H.; Heo, J. H.; Mandal, T. N.; Seok, S. Il. Chemical Management for Colorful, Efficient, and Stable Inorganic−Organic Hybrid Nanostructured Solar Cells. *Nano Lett.* **2013**, *13*, 1764−1769.

(7) Protesescu, L.; Yakunin, S.; Bodnarchuk, M. I.; Krieg, F.; Caputo, R.; Hendon, C. H.; Yang, R. X.; Walsh, A.; Kovalenko, M. V. Nanocrystals of Cesium Lead Halide Perovskites ($CsPbX_3$, X = Cl, Br, and I): Novel Optoelectronic Materials Showing Bright Emission with Wide Color Gamut. *Nano Lett.* **2015**, *15*, 3692−3696.

(8) Eperon, G. E.; Leijtens, T.; Bush, K. A.; Prasanna, R.; Green, T.; Wang, J. T.-W.; McMeekin, D. P.; Volonakis, G.; Milot, R. L.; May, R.; et al. Perovskite-Perovskite Tandem Photovoltaics with Optimized Band Gaps. *Science* **2016**, *354*, 861−865.

(9) Zhao, D.; Yu, Y.; Wang, C.; Liao, W.; Shrestha, N.; Grice, C. R.; Cimaroli, A. J.; Guan, L.; Ellingson, R. J.; Zhu, K.; et al. Low-Bandgap Mixed Tin−Lead Iodide Perovskite Absorbers with Long Carrier Lifetimes for All-Perovskite Tandem Solar Cells. *Nat. Energy* **2017**, *2*, 17018.

(10) Tong, J.; Song, Z.; Kim, D. H.; Chen, X.; Chen, C.; Palmstrom, A. F.; Ndione, P. F.; Reese, M. O.; Dunfield, S. P.; Reid, O. G.; et al. Carrier Lifetimes of > 1 μs in Sn-Pb Perovskites Enable Efficient All-Perovskite Tandem Solar Cells. *Science* **2019**, *364*, 475−479.

(11) Lin, R.; Xiao, K.; Qin, Z.; Han, Q.; Zhang, C.; Wei, M.; Saidaminov, M. I.; Gao, Y.; Xu, J.; Xiao, M.; et al. Monolithic All-Perovskite Tandem Solar Cells with 24.8% Efficiency Exploiting Comproportionation to Suppress Sn(II) Oxidation in Precursor Ink. *Nat. Energy* **2019**, *4*, 864−873.

(12) Tong, J.; Jiang, Q.; Ferguson, A. J.; Palmstrom, A. F.; Wang, X.; Hao, J.; Dunfield, S. P.; Louks, A. E.; Harvey, S. P.; Li, C.; et al. Carrier Control in Sn−Pb Perovskites via 2D Cation Engineering for All-Perovskite Tandem Solar Cells with Improved Efficiency and Stability. *Nat. Energy* **2022**, *7*, 642−651.

(13) Abdollahi Nejand, B.; Ritzer, D. B.; Hu, H.; Schackmar, F.; Moghadamzadeh, S.; Feeney, T.; Singh, R.; Laufer, F.; Schmager, R.; Azmi, R.; et al. Scalable Two-Terminal All-Perovskite Tandem Solar Modules with a 19.1% Efficiency. *Nat. Energy* **2022**, *7*, 620−630.

(14) Wang, C.; Zhao, Y.; Ma, T.; An, Y.; He, R.; Zhu, J.; Chen, C.; Ren, S.; Fu, F.; Zhao, D.; et al. A Universal Close-Space Annealing Strategy towards High-Quality Perovskite Absorbers Enabling Efficient All-Perovskite Tandem Solar Cells. *Nat. Energy* **2022**, *7*, 744−753.

(15) Han, Q.; Hsieh, Y.-T.; Meng, L.; Wu, J.-L.; Sun, P.; Yao, E.-P.; Chang, S.-Y.; Bae, S.-H.; Kato, T.; Bermudez, V.; et al. High-Performance Perovskite/Cu(In,Ga)Se$_2$ Monolithic Tandem Solar Cells. *Science* **2018**, *361*, 904−908.

(16) Jošt, M.; Köhnen, E.; Al-Ashouri, A.; Bertram, T.; Tomšič, Š.; Magomedov, A.; Kasparavicius, E.; Kodalle, T.; Lipovšek, B.; Getautis, V.; et al. Perovskite/CIGS Tandem Solar Cells: From Certified 24.2% toward 30% and Beyond. *ACS Energy Lett.* **2022**, *7*, 1298−1307.

(17) Brinkmann, K. O.; Becker, T.; Zimmermann, F.; Kreusel, C.; Gahlmann, T.; Theisen, M.; Haeger, T.; Olthof, S.; Tückmantel, C.; Günster, M.; et al. Perovskite−Organic Tandem Solar Cells with Indium Oxide Interconnect. *Nature* **2022**, *604*, 280−286.

(18) Bush, K. A.; Palmstrom, A. F.; Yu, Z. J.; Boccard, M.; Cheacharoen, R.; Mailoa, J. P.; McMeekin, D. P.; Hoye, R. L. Z.; Bailie, C. D.; Leijtens, T.; et al. 23.6%-Efficient Monolithic Perovskite/Silicon Tandem Solar Cells with Improved Stability. *Nat. Energy* **2017**, *2*, 17009.

(19) Sahli, F.; Werner, J.; Kamino, B. A.; Bräuninger, M.; Monnard, R.; Paviet-Salomon, B.; Barraud, L.; Ding, L.; Diaz Leon, J. J.; Sacchetto, D.; et al. Fully Textured Monolithic Perovskite/Silicon Tandem Solar Cells with 25.2% Power Conversion Efficiency. *Nat. Mater.* **2018**, *17*, 820−826.

(20) Xu, J.; Boyd, C. C.; Yu, Z. J.; Palmstrom, A. F.; Witter, D. J.; Larson, B. W.; France, R. M.; Werner, J.; Harvey, S. P.; Wolf, E. J.; et al. Triple-Halide Wide-Band Gap Perovskites with Suppressed Phase Segregation for Efficient Tandems. *Science* **2020**, *367*, 1097−1104.

(21) Al-Ashouri, A.; Köhnen, E.; Li, B.; Magomedov, A.; Hempel, H.; Caprioglio, P.; Márquez, J. A.; Morales Vilches, A. B.; Kasparavicius, E.; Smith, J. A.; et al. Monolithic Perovskite/Silicon Tandem Solar Cell with > 29% Efficiency by Enhanced Hole Extraction. *Science* **2020**, *370*, 1300−1309.

(22) Hou, Y.; Aydin, E.; De Bastiani, M.; Xiao, C.; Isikgor, F. H.; Xue, D.-J.; Chen, B.; Chen, H.; Bahrami, B.; Chowdhury, A. H.; et al. Efficient Tandem Solar Cells with Solution-Processed Perovskite on Textured Crystalline Silicon. *Science* **2020**, *367*, 1135−1140.

(23) Liu, J.; De Bastiani, M.; Aydin, E.; Harrison, G. T.; Gao, Y.; Pradhan, R. R.; Eswaran, M. K.; Mandal, M.; Yan, W.; Seitkhan, A.; et al. Efficient and Stable Perovskite-Silicon Tandem Solar Cells through Contact Displacement by MgF$_X$. *Science* **2022**, *377*, 302−306.

(24) Lin, R.; Xu, J.; Wei, M.; Wang, Y.; Qin, Z.; Liu, Z.; Wu, J.; Xiao, K.; Chen, B.; Park, S. M.; et al. All-Perovskite Tandem Solar Cells with Improved Grain Surface Passivation. *Nature* **2022**, *603*, 73−78.

(25) Green, M. A.; Dunlop, E. D.; Hohl-Ebinger, J.; Yoshita, M.; Kopidakis, N.; Bothe, K.; Hinken, D.; Rauer, M.; Hao, X. Solar Cell Efficiency Tables (Version 60). *Prog. Photovoltaics Res. Appl.* **2022**, *30*, 687−701.

(26) Li, L.; Wang, Y.; Wang, X.; Lin, R.; Luo, X.; Liu, Z.; Zhou, K.; Xiong, S.; Bao, Q.; Chen, G.; et al. Flexible All-Perovskite Tandem Solar Cells Approaching 25% Efficiency with Molecule-Bridged Hole-Selective Contact. *Nat. Energy* **2022**, *7*, 708−717.

(27) Kothandaraman, R. K.; Jiang, Y.; Feurer, T.; Tiwari, A. N.; Fu, F. Near-Infrared-Transparent Perovskite Solar Cells and Perovskite-Based Tandem Photovoltaics. *Small Methods* **2020**, *4*, 2000395.

(28) Jošt, M.; Kegelmann, L.; Korte, L.; Albrecht, S. Monolithic Perovskite Tandem Solar Cells: A Review of the Present Status and Advanced Characterization Methods Toward 30% Efficiency. *Adv. Energy Mater.* **2020**, *10*, 1904102.

(29) Fu, F.; Feurer, T.; Weiss, T. P.; Pisoni, S.; Avancini, E.; Andres, C.; Buecheler, S.; Tiwari, A. N. High-Efficiency Inverted Semi-Transparent Planar Perovskite Solar Cells in Substrate Configuration. *Nat. Energy* **2017**, *2*, 16190.

(30) Feleki, B. T.; Chandrashekar, S.; Bouwer, R. K. M.; Wienk, M. M.; Janssen, R. A. J. Development of a Perovskite Solar Cell Architecture for Opaque Substrates. *Sol. RRL* **2020**, *4*, 2000385.

(31) Feleki, B. T.; Bouwer, R. K. M.; Zardetto, V.; Wienk, M. M.; Janssen, R. A. J. p−i−n Perovskite Solar Cells on Steel Substrates. *ACS Appl. Energy Mater.* **2022**, *5*, 6709−6715.

(32) Wojciechowski, K.; Forgács, D.; Rivera, T. Industrial Opportunities and Challenges for Perovskite Photovoltaic Technology. *Sol. RRL* **2019**, *3*, 1900144.

(33) Werner, J.; Boyd, C. C.; Moot, T.; Wolf, E. J.; France, R. M.; Johnson, S. A.; van Hest, M. F. A. M.; Luther, J. M.; Zhu, K.; Berry, J. J.; et al. Learning from Existing Photovoltaic Technologies to Identify Alternative Perovskite Module Designs. *Energy Environ. Sci.* **2020**, *13*, 3393−3403.

(34) Song, Z.; Li, C.; Chen, L.; Yan, Y. Perovskite Solar Cells Go Bifacial—Mutual Benefits for Efficiency and Durability. *Adv. Mater.* **2022**, *34*, 2106805.

(35) Hu, S.; Otsuka, K.; Murdey, R.; Nakamura, T.; Truong, M. A.; Yamada, T.; Handa, T.; Matsuda, K.; Nakano, K.; Sato, A.; et al. Optimized Carrier Extraction at Interfaces for 23.6% Efficient Tin−

Lead Perovskite Solar Cells. *Energy Environ. Sci.* **2022**, *15*, 2096–2107.

(36) Zanoni, K. P. S.; Paliwal, A.; Hernández-Fenollosa, M. A.; Repecaud, P.; Morales-Masis, M.; Bolink, H. J. ITO Top-Electrodes via Industrial-Scale PLD for Efficient Buffer-Layer-Free Semitransparent Perovskite Solar Cells. *Adv. Mater. Technol.* **2022**, *7*, 2101747.

(37) Kaya, I. C.; Zanoni, K. P. S.; Palazon, F.; Sessolo, M.; Akyildiz, H.; Sonmezoglu, S.; Bolink, H. J. Crystal Reorientation and Amorphization Induced by Stressing Efficient and Stable P–I–N Vacuum-Processed MAPbI$_3$ Perovskite Solar Cells. *Adv. Energy Sustainability Res.* **2021**, *2*, 2000065.

(38) Longo, G.; Momblona, C.; La-Placa, M.-G.; Gil-Escrig, L.; Sessolo, M.; Bolink, H. J. Fully Vacuum-Processed Wide Band Gap Mixed-Halide Perovskite Solar Cells. *ACS Energy Lett.* **2018**, *3*, 214–219.

(39) Momblona, C.; Gil-Escrig, L.; Bandiello, E.; Hutter, E. M.; Sessolo, M.; Lederer, K.; Blochwitz-Nimoth, J.; Bolink, H. J. Efficient Vacuum Deposited p-i-n and n-i-p Perovskite Solar Cells Employing Doped Charge Transport Layers. *Energy Environ. Sci.* **2016**, *9*, 3456–3463.

(40) van Reenen, S.; Kemerink, M.; Snaith, H. J. Modeling Anomalous Hysteresis in Perovskite Solar Cells. *J. Phys. Chem. Lett.* **2015**, *6*, 3808–3814.

(41) Calado, P.; Telford, A. M.; Bryant, D.; Li, X.; Nelson, J.; O'Regan, B. C.; Barnes, P. R. F. Evidence for Ion Migration in Hybrid Perovskite Solar Cells with Minimal Hysteresis. *Nat. Commun.* **2016**, *7*, 13831.

(42) Forgács, D.; Gil-Escrig, L.; Pérez-Del-Rey, D.; Momblona, C.; Werner, J.; Niesen, B.; Ballif, C.; Sessolo, M.; Bolink, H. J. Efficient Monolithic Perovskite/Perovskite Tandem Solar Cells. *Adv. Energy Mater.* **2017**, *7*, 1602121.

(43) Ávila, J.; Momblona, C.; Boix, P.; Sessolo, M.; Anaya, M.; Lozano, G.; Vandewal, K.; Míguez, H.; Bolink, H. J. High Voltage Vacuum-Deposited CH$_3$NH$_3$PbI$_3$–CH$_3$NH$_3$PbI$_3$ Tandem Solar Cells. *Energy Environ. Sci.* **2018**, *11*, 3292–3297.

(44) Oviedo, F.; Liu, Z.; Ren, Z.; Thway, M.; Buonassisi, T.; Peters, I. M. Ohmic Shunts in Two-Terminal Dual-Junction Solar Cells with Current Mismatch. *Jpn. J. Appl. Phys.* **2017**, *56*, 08MA05.